

Mesoscopic Correlation with Polarization of Electromagnetic Waves

A.A. Chabanov,^{1,*} N.P. Trégourès,² B.A. van Tiggelen,² and A.Z. Genack¹

¹*Department of Physics, Queens College of the City University of New York, Flushing, NY 11367, USA*

²*Laboratoire de Physique et Modélisation des Milieux Condensés,
CNRS/Université Joseph Fourier, Maison des Magistères, B.P. 166, 38042 Grenoble, France*
(Dated: September 4, 2003)

Mesoscopic correlations are observed in the polarization of microwave radiation transmitted through a random waveguide. These measurements, supported by diagrammatic theory, permit the unambiguous identification of short, long, and infinite range components in the intensity correlation function, as well as an additional frequency-independent component.

PACS numbers: 42.25.Dd, 42.25.Ja

Mesoscopic transport of both classical and quantum mechanical waves is characterized by the degree of non-local intensity or current correlation which reflects the closeness to the Anderson localization threshold [1, 2]. Correlation is generally treated using scalar waves with the electromagnetic (EM) polarization or electron spin accounted for by doubling the density of states. The vector nature of EM radiation is exhibited in coherent backscattering [3], the photon Hall effect [4], and the memory of rotation of incident polarization [5]. These polarization effects reflect short-range field correlation and can be obtained within the field factorization approximation applicable to Gaussian statistics, as opposed to mesoscopic intensity correlation.

In this Letter, we present measurements and calculations of intensity correlation with polarization rotation that go beyond the field factorization approximation. Polarization is thereby shown to be an essential mesoscopic variable complementary to space, frequency, and time. Unlike these variables, however, the polarization variable is of finite range with only two independent values. Consequently, the field correlation function with polarization rotation has a simple form independent of scattering strength. It is determined exclusively by the cosine of the angular shifts in the polarization of the electric field at the source and detector and vanishes when either polarization is shifted by 90° . This enables an unambiguous separation of the intensity correlation function, C , into short (C_1) [6, 7], long (C_2) [8, 9], and infinite (C_3) [10, 11, 12] range components, which determine fluctuations in intensity, total transmission, and conductance, respectively. The frequency correlation function of each of these universal components can thereby be found. In addition, the presence of a frequency-independent component is identified. This term may correspond to a nonuniversal “ C_0 ” contribution, which reflects the scattering environment at the input and output surfaces [13].

We begin with the conjecture, borne out by diagrammatic calculations and measurements reported below, that the structure of the correlation function of normalized intensity with regard to rotations in the polarization of source and detector, $C(\Delta\theta_S, \Delta\theta_D)$, is analogous

to that of the correlation function with displacement of the source and detector, $C(\Delta\mathbf{r}_S, \Delta\mathbf{r}_D)$ [14]. In each component, C depends upon a given degree of freedom only through its dependence upon the square of the field correlation function, $F \equiv |F_E|^2$. When expressed in terms of polarization rotations of the source and detector, this gives,

$$\begin{aligned} C(\Delta\theta_S, \Delta\theta_D) &= F(\Delta\theta_S)F(\Delta\theta_D) \\ &+ A'_2[F(\Delta\theta_S) + F(\Delta\theta_D)] \\ &+ A'_3[1 + F(\Delta\theta_S) + F(\Delta\theta_D) \\ &\quad + F(\Delta\theta_S)F(\Delta\theta_D)]. \end{aligned} \quad (1)$$

The leading contributions to A'_2 and A'_3 are of order $1/g$ and $1/g^2$, respectively, where g is the dimensionless conductance.

The field correlation function with polarization rotation can readily be found for multiply scattered waves when the transmitted field is completely depolarized. In this case, the average intensity is independent of the polarization of the field at the source or detector and cross-polarized fields are uncorrelated. When the polarization of the detector is rotated by $\Delta\theta_D$ from an initial direction θ_D , the detected field $\mathbf{E}(\theta_D + \Delta\theta_D)$ may be expressed in terms of the vector sum of the field along θ_D , $\mathbf{E}(\theta_D)$, and the field perpendicular to this direction, $\mathbf{E}(\theta_D + 90^\circ)$, as follows, $\mathbf{E}(\theta_D + \Delta\theta_D) = \mathbf{E}(\theta_D) \cos \Delta\theta_D + \mathbf{E}(\theta_D + 90^\circ) \sin \Delta\theta_D$. The field correlation function for the normalized average intensity, $\langle |\mathbf{E}(\theta_D)|^2 \rangle = 1$, is therefore, $F_E(\Delta\theta_D) \equiv \langle \mathbf{E}(\theta_D) \mathbf{E}^*(\theta_D + \Delta\theta_D) \rangle = \cos \Delta\theta_D$. Here $\langle \dots \rangle$ denotes the average over an ensemble of realizations. A similar argument gives the field correlation function of the detected field when the source polarization is rotated by $\Delta\theta_S$, $F_E(\Delta\theta_S) = \cos \Delta\theta_S$. The total field correlation function with polarization rotation is therefore given by $F_E(\Delta\theta_S, \Delta\theta_D) = F_E(\Delta\theta_S)F_E(\Delta\theta_D) = \cos \Delta\theta_S \cos \Delta\theta_D$.

The contributions to C in Eq. (1) can be expressed in terms of the product or sum of $F(\Delta\theta_S)$ and $F(\Delta\theta_D)$ or of a constant. Since these three types of terms are associated, respectively, with short, long, and infinite range correlation, it is convenient to group these terms sepa-

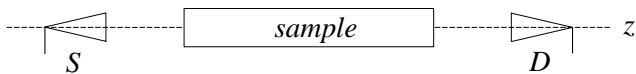


FIG. 1: Schematics of the experimental setup: S (source) and D (detector) microwave horns are positioned symmetrically in front and behind the sample and can be rotated about their axes (z -axis) thus rotating the polarizations of the incident and detected waves.

rately. We therefore write,

$$C(\Delta\theta_S, \Delta\theta_D) = (1 + A_1) \cos^2 \Delta\theta_S \cos^2 \Delta\theta_D + A_2 (\cos^2 \Delta\theta_S + \cos^2 \Delta\theta_D) + A_3. \quad (2)$$

For the case, in which nonuniversal “ C_0 ” contributions to C are negligible, $A_1 = A'_3$, $A_2 = A'_2 + A'_3$, and $A_3 = A'_3$. The analysis of Ref. [14] has been generalized to vector waves in a detailed diagrammatic study [15]. The relation $A_1 = A_3$, which follows from Eq. (1), can be understood from the topological structure of the underlying diagrams, and the equal weights of the two A_2 terms follow from reciprocity. In the diffusive regime in the absence of absorption, to order $1/g^2$,

$$A'_2 = \frac{2}{3} \frac{1}{g}, \quad A'_3 = \frac{2}{15} \frac{1}{g^2}, \quad (3)$$

where $g = 2 \times Ak^2\ell/3\pi L$, which includes both polarizations. Here, k is the wave number, ℓ is the transport mean free path, A and L are the cross-section area and length of the sample, respectively. Values of A'_2 and A'_3 slightly depend on absorption [14, 17, 18]. In our experiment, $L/L_a = 3.6$, where L_a is the absorption length. This gives $A'_2 = 0.57/g$ and $A'_3 = 0.113/g^2$.

Measurements of the dependence of the field and intensity correlation functions upon polarization rotation for microwave radiation transmitted through a random dielectric sample are made with identical conical horns positioned 40 cm in front and behind the sample (Fig. 1). Linearly polarized microwave radiation is launched from horn S and a linearly polarized component of the transmitted field is captured by horn D . The polarization of incident and detected waves can be rotated in the xy -plane by rotating the corresponding horn about its axis (z -axis). Because of the conical shape of the horns, the angular distribution of the incident and detected radiation do not depend strongly on the rotation of the horns. As a result, the variation in the detected field at a given frequency for a given sample realization is mainly due to the shift in the polarization of the field at the source and detector. The sample is composed of 0.95-cm-diameter alumina spheres with refractive index 3.14 embedded within Styrofoam spheres of diameter 1.9 cm and refractive index 1.04. The sample with an alumina volume fraction of 0.068 is contained in a 7.3-cm-diameter copper tube

of length $L = 90$ cm. Measurements for random ensembles are obtained by momentarily rotating the sample tube about its axis to create new sample realizations, after which spectra are taken for each orientation of the polarizers. Measurements are carried out in an ensemble of 12,000 sample realizations for 2 orientations of the source polarizer rotated by 90° and 7 orientations of the detector polarizer rotated in steps of 15° , and also in an ensemble of 32,000 realizations for 2 orientations of each polarizer rotated by 90° . The transmitted field is measured in steps of 1 MHz from 16.95 to 17.05 GHz using a Hewlett-Packard 8772C vector network analyzer. This frequency range is centered at the peak of the fourth Mie resonance of the alumina spheres [16] and is much narrower than the width of the resonance so that propagation parameters within this range are nearly constant. At $\nu = 17$ GHz, the number of transverse channels in the sample tube is $N = Ak^2/2\pi = 84$. The transport mean free path estimated from Mie theory is $\ell = 2.34$ cm, giving $g \approx 4N\ell/3L = 2.91$. A fit of diffusion theory to the measured field correlation function with frequency shift gives $D = 8.0$ cm²/ns for the diffusion coefficient and $L_a = 24.9$ cm for the absorption length.

The real and imaginary parts of $F_E(0, \Delta\theta_D)$ obtained by averaging over frequency for an ensemble of 12,000 sample configurations are displayed by the crosses in Figs. 2a and 2b, respectively. The dashed curves represent the predictions — $\cos \Delta\theta_D$ for the real part and 0 for the imaginary part. The orientation of the horn polarizations for the initial and final data points are indicated by the arrows. In addition, we find $F_E(90, \Delta\theta_D)$ to vanish for all the values of $\Delta\theta_D$. Though the measurements are consistent with the predicted behavior of F_E , there is an increasing systematic deviation from theory with increasing $\Delta\theta_S$ or $\Delta\theta_D$. This deviation arises because, in addition to rotation of the polarization, there is a residual variation of the spatial intensity distribution on the sample, as the horn is rotated.

The intensity correlation functions $C(0, \Delta\theta_D)$ and $C(90, \Delta\theta_D)$ for the same data set are shown by the blue crosses in Figs. 3a and 3b, respectively. In addition, $F(\Delta\theta_D)$ is shown in Fig. 3a by the red crosses, which lie close to the solid curve of $\cos^2 \Delta\theta_D$. A Legendre polynomial fit of $C(0, \Delta\theta_D)$ and $C(90, \Delta\theta_D)$ shows that, with high accuracy, they are of the form $a + b \cos^2 \Delta\theta_D$, where a and b are constants, in agreement with Eq. (2). The dashed curve in Fig. 3a is a fit to the first 4 data points of $C(0, \Delta\theta_D)$ of the function $a + b \cos^2 \Delta\theta_D$, where $a = A_2 + A_3$ and $b = 1 + A_1 + A_2$. Only the first four points are used because the systematic deviation in C due to the redistribution of intensity with rotation cannot be ignored for larger polarization rotations. Though uncertainty is introduced into C_1 and C_2 by the horn rotation, there is no such effect on C_3 because it is independent of both polarization and displacement. Thus the measured value for A_3 is not affected by the horn rotation. It is

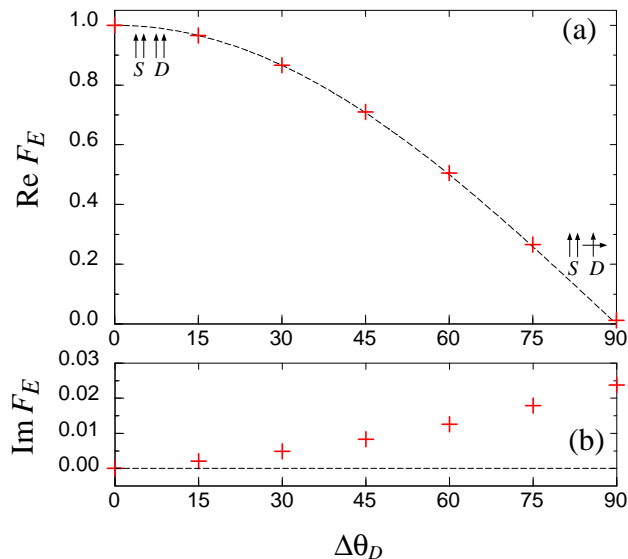


FIG. 2: (a) Real and (b) imaginary parts of the field correlation function $F_E(0, \Delta\theta_D)$ plotted versus the angular shift of the polarization of the detected field, $\Delta\theta_D$, as the polarization of the incident wave is kept unchanged, $\Delta\theta_S = 0$. The arrows indicate orientations of the source (S) and detector (D) polarizers for the initial and final data points. The dashed lines represent the theoretical prediction, $F_E(0, \Delta\theta_D) = \cos(\Delta\theta_D)$.

found directly from $C(90, 90)$ for an ensemble of 44,000 realizations, $A_3 = 0.029 \pm 0.001$. From the fit, we obtain $A_1 + A_2 = 0.286 \pm 0.005$ and $A_2 + A_3 = 0.293 \pm 0.004$. Hence $A_2 = 0.264 \pm 0.006$ and $A_1 = 0.022 \pm 0.010$. The dashed curve in Fig. 3b is $A_3 + A_2 \cos^2 \Delta\theta_D$ with the A_2 and A_3 found above. The difference between the experimental data points and the curve represents the loss of correlation due to the redistribution of intensity with the horn rotation.

The coefficients A_i for arbitrary frequency shift can be determined from spectral measurements for three orientations of the source and detector as follows, $A_3 = C(90, 90)$, $A_2 = C(0, 90) - A_3$, and $A_1 = C(0, 0) - |F_E(0, 0)|^2 - 2A_2 - A_3$. We have utilized the above procedure in the ensemble of 44,000 sample realizations, to find $A_i(\Delta\nu)$ for frequency shifts $\Delta\nu$ up to 100 MHz, that is almost 100 times the Thouless frequency $\Delta\nu_{Th} \equiv 6D/2\pi L^2 \approx 1$ MHz. To compensate for the loss of correlation in $C(0, 90)$ due to the redistribution of intensity, the corresponding frequency correlation function was multiplied by a constant to make it equal to the $A_2 + A_3$ at zero frequency shift. The resulting dependencies are shown by the squares in Fig. 4. $A_2(\Delta\nu)$ and $A_3(\Delta\nu)$ are predicted [17] to fall asymptotically as $A_2(\Delta\nu) \sim 1/(\Delta\nu)^{1/2}$ and $A_3(\Delta\nu) \sim 1/(\Delta\nu)^{3/2}$. We find, however, that A_3 exhibits a *nonzero* correlation for $\Delta\nu \gg \Delta\nu_{Th}$, that largely exceeds error bars, and that A_2 is shifted from the predicted curve by a nearly constant

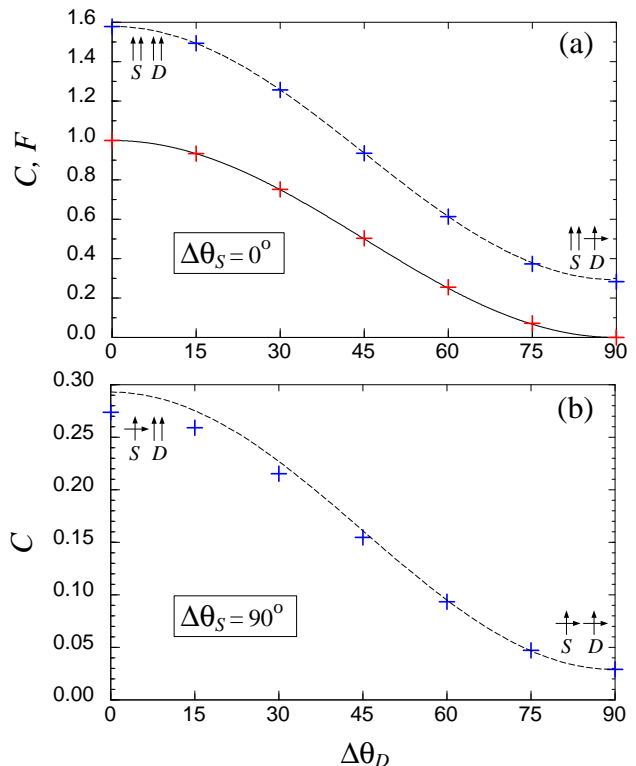


FIG. 3: (a) Intensity correlation functions C and F plotted versus $\Delta\theta_D$ for $\Delta\theta_S = 0$. The solid line is the prediction, $F(\Delta\theta_D) = \cos^2(\Delta\theta_D)$. The dashed line is the fit of $C(0, \Delta\theta_D)$ to the first 4 data points. (b) C versus $\Delta\theta_D$ for $\Delta\theta_S = 90^\circ$. The dashed line is the prediction $A_3 + A_2 \cos^2 \Delta\theta_D$ with the A_2 and A_3 found from the fit in (a).

value. Figs. 4a and 4b show that agreement with theory is obtained for $A_{2,3}$, if *frequency-independent* contributions with the values $A_2(\infty) = -0.015$ and $A_3(\infty) = 0.007$ are incorporated, respectively, in A_2 and A_3 . We do not observe an asymptotic background in A_1 (Fig. 4c). The observed $A_1(\Delta\nu)$, however, falls faster than predicted by diagrammatic theory. To calculate $A_1(\Delta f)$, we have modified the theory for $A_3(\Delta f)$ [17].

After subtracting the asymptotic values we find $A_3(0) - A_3(\infty) = A'_3(0) = 0.022 \pm 0.001$ and $A_2(0) - A_2(\infty) = A'_2(0) + A'_3(0) = 0.279 \pm 0.004$ at zero frequency shift. Note that $A'_3(0) = A_1(0)$ holds within the error bars. Using Eq. (3) the value for $A'_3(0)$ yields $g = 2.27 \pm 0.05$ for the dimensionless conductance. This differs from the estimate, reflecting effects of localization, internal reflection, and finite scatterer density. Using this value, Eq. (3) predicts $A'_2(0) = 0.252$, and hence $A'_2(0) + A'_3(0) = 0.274$, which is also consistent with observations.

It is tempting to associate the frequency-independent background term with the C_0 term of Ref. [13]. A preliminary calculation for point dipoles in a tube geometry with N transverse channels [19] shows C_0 to be

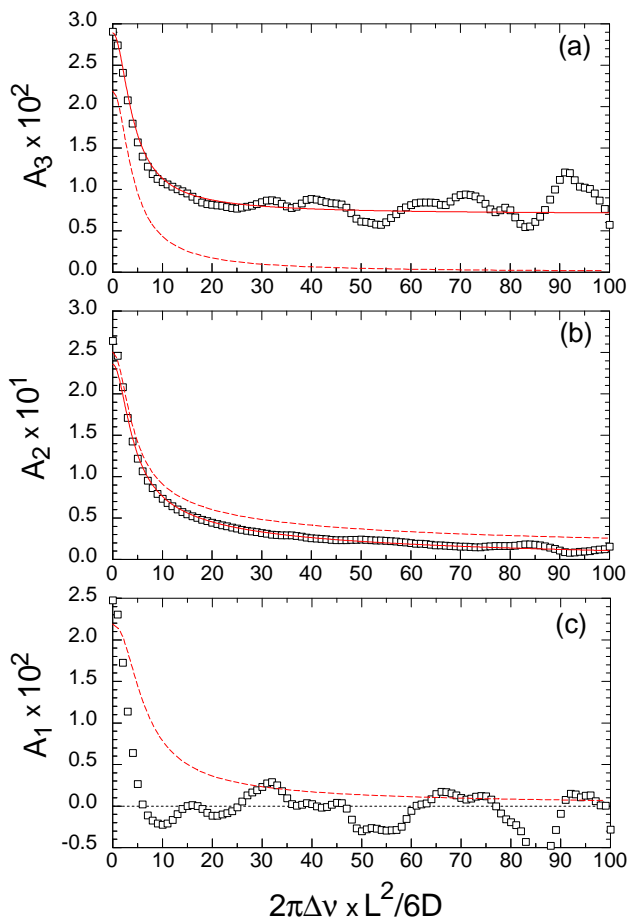


FIG. 4: Coefficients A_3 (a), A_2 (b), and A_1 (c) plotted versus frequency shift. The long-dashed curves represent predictions of mesoscopic theory [17] for A_3 (a), A_2' (b), and A_1 (c) with $g = 2.27$ and $L/L_a = 3.6$. The frequency-independent contributions with the values $A_3(\infty) = 0.007$ and $A_2(\infty) = -0.015$ have been added, respectively, to the predicted A_3 and A_2' to obtain the solid curves and agreement with the data.

independent of frequency shift, positive and of order $1/N = 0.012$, and with contributions to A_2 and A_3 and not to A_1 . This is consistent with the observed value $A_3(\infty) = 0.007$, but not with the *negative* value $A_2(\infty) = -0.015$. A vector Mie theory for C_0 along with measurements in samples with different longitudinal and transverse dimensions may shed light on this issue.

In conclusion, mesoscopic correlations have been found in the polarization of microwave radiation transmitted through a random waveguide. The intensity correlation function with polarization rotation is shown to be composed of the product and sum of the square of the field correlation function and of a constant term. These three types of terms are associated, respectively, with short, long, and infinite range correlation. The variation with frequency shift of each of these terms has been measured. The long and infinite range terms are found to include

a frequency-independent component, which may be related to the short-duration interaction of the wave with regions of limited spatial extent near the input and output surfaces of the sample. The simple form of the three contributions to the intensity correlation function with polarization rotation allows an unambiguous separation of correlation into short, long, and infinite range contributions. This method is readily applicable to optical measurements and can be used to determine the degree of intensity correlation in a sample and hence the closeness to the localization threshold. Analogous correlations can also be expected in electron spin propagating in a random potential.

It is a pleasure to acknowledge stimulating discussions with R. Pnini, S.E. Skipetrov, and B. Shapiro. We would also like to thank G. German and Z. Ozimkowski for help in constructing the experimental apparatus, as well as K. Chabanov and B. Hu for experimental assistance. This research is sponsored by the U.S. Army Research Office (DAAD190010362), the National Science Foundation (DMR0205186), and GDR 2253 IMCODE of the CNRS.

* Present address: CEMS, University of Minnesota, Minneapolis, MN 55545, USA

- [1] *Scattering and Localization of Classical Waves in Random Media*, edited by Ping Sheng (World Scientific, Singapore, 1990).
- [2] *Mesoscopic Phenomena in Solids*, edited by B.L. Altshuler, P.A. Lee, and R.A. Webb (North Holland, Amsterdam, 1991).
- [3] M.P. van Albada and A. Lagendijk, Phys. Rev. Lett. **55**, 2692 (1985); P.E. Wolf and G. Maret, Phys. Rev. Lett. **55**, 2696 (1985); E. Akkermans, P.E. Wolf, and R. Maynard, Phys. Rev. Lett. **56**, 1471 (1986).
- [4] G.L.J.A. Rikken and B.A. van Tiggelen, Nature **381**, 54 (1996).
- [5] I. Freund, M. Kaveh, R. Berkovits, and M. Rosenbluh, Phys. Rev. B **42**, 2613 (1990).
- [6] B. Shapiro, Phys. Rev. Lett. **57**, 2168 (1986).
- [7] I. Freund, M. Rosenbluh, and S. Feng, Phys. Rev. Lett. **61**, 2328 (1988).
- [8] M.J. Stephen and G. Cwilich, Phys. Rev. Lett. **59**, 285 (1987).
- [9] A.Z. Genack, N. Garcia, and W. Polkosnik, Phys. Rev. Lett. **65**, 2129 (1990); J.F. de Boer, M.P. van Albada and A. Lagendijk, Phys. Rev. B **45**, 658 (1992).
- [10] R.A. Webb, S. Washburn, C.P. Umbach, and R.B. Laibowitz, Phys. Rev. Lett. **54**, 2696 (1985); B.L. Altshuler and D.E. Khmelnitskii, JETP Lett. **42**, 359 (1985); P.A. Lee and A.D. Stone, Phys. Rev. Lett. **55**, 1622 (1985).
- [11] S. Feng, C. Kane, P.A. Lee, and A.D. Stone, Phys. Rev. Lett. **61**, 834 (1988).
- [12] F. Scheffold and G. Maret, Phys. Rev. Lett. **81**, 5800 (1998).
- [13] B. Shapiro, Phys. Rev. Lett. **83**, 4733 (1999); S.E. Skipetrov and R. Maynard, Phys. Rev. B **62**, 886

- (2000).
- [14] R. Pnini, in *Waves and Imaging Through Complex Media*, edited by P. Sebbah (Kluwer Academic, Dordrecht, 2001); P. Sebbah, B. Hu, A.Z. Genack, R. Pnini, and B. Shapiro, Phys. Rev. Lett. **88**, 123901 (2002).
 - [15] N. Trégourès, *Approche Mésooscopique des Ondes en Milieu Complexe: des Micro-ondes aux Ondes Sismiques*, Ph.D thesis, University of Grenoble 1 (2001).
 - [16] A.A. Chabanov and A.Z. Genack, Phys. Rev. Lett. **87**, 153901 (2001).
 - [17] M.C.W. van Rossum and Th.M. Nieuwenhuizen, Rev. Mod. Phys. **71**, 313 (1999).
 - [18] P.W. Brouwer, Phys. Rev. B **57**, 10526 (1998).
 - [19] S.E. Skipetrov, unpublished.